JCAMECH

Vol. 51, No. 2, December 2020, pp 389-402
DOI: 10.22059/jcamech.2020.303972.516

A hybrid scheme of single relaxation time lattice Boltzmann and finite volume methods coupled with discrete ordinates method for combined natural convection and volumetric radiation in an enclosure

Rabiaa Soualmi [a] ∗, Abderrahmane Benbrik [a], Denis Lemonnier[b], Mohammed Cherifi [a] and Mohammed Bouanani [a]

[a] *Laboratory of Petroleum Equipments Reliability and Materials, Université M'Hamed Bougara, Boumerdés, Algerie*
[b] *Institut Pprime, CNRS, ENSMA, University of Poitiers, Poitiers, 86961 Chasseneuil Futuroscope, France*

ARTICLE INFO

Article history:
Received:12 June 2020
Accepted: 12 July 2020

Keywords:
Natural convection
Volumetric radiation
Single relaxation time lattice Boltzmann method
Aspect ratio
Discrete ordinates method

ABSTRACT

This paper is focused on the application of hybrid Single relaxation time lattice Boltzmann and finite volume methods in conjunction with discrete ordinates method to simulate coupled natural convection and volumetric radiation in differentially heated enclosure, filled with an absorbing, emitting and non-scattering gray medium. In this work, the velocity and temperature fields are calculated using lattice Boltzmann and finite volume methods respectively, whereas the radiative term is computed by the discrete ordinates method. This study is carried out for Pr = 0.71, a Rayleigh number range of $10^3 \leq Ra \leq 10^6$, an optical thickness with values $0 \leq \tau \leq 100$, a Planck number ranging in $0.001 \leq Pl \leq 100$ and an aspect ratio varying between $0.5 \leq Ar \leq 2$. Results are presented in terms of streamlines, isotherms, velocity profiles and average Nusselt number. Based on the obtained results, it can be concluded that the presence of volumetric radiation is noteworthy. Its effect, as a function of Rayleigh number and the radiative properties, yields significant changes on the behavior of streamlines and isotherms. In the taller enclosure, the increase of average total Nusselt number with increasing Rayleigh number is less significant than that in the case of the shallow enclosure.

1. Introduction

Natural convection problem in an enclosure has been a very important subject in the active research. This is due to its relevance to several technological applications, including industrial furnaces and boilers, cooling of electronic equipments, thermal energy storage, heat exchangers, processes involving high temperature and many others. The radiation phenomenon in participating media can strongly interfere with such problem in many cases of the aforementioned applications. Therefore, several researchers showed interest in studying the interaction of natural convection and volumetric radiation in an enclosure containing a participating medium. In order to solve the latter problem, various numerical methods have been commonly employed in the recent years, such as the conventional computation fluid dynamics methods (finite difference (FD), finite volume (FV) and finite elements (FE) methods), the lattice Boltzmann method (LBM) and the combination of both.

Among these numerical methods, the LBM has recently attracted a great attention from numerous investigators in the recent years and has been considered as one of the best alternative to CFD techniques. It has also achieved an appreciable success in the hybrid schemes (meaning, coupled of CFD and LB methods). Contrary to the conventional CFD methods, which are based on the discretization of macroscopic continuum equations, the LBM uses the microscopic model and mesoscopic kinetic equations. The LBM presents many advantages, including the easy implementation of the boundary conditions, a fully parallel algorithm, the ease of the discretization process and the gain in computation time [1, 2] .

* Corresponding author. Tel.: +213 663 70 70 36; e-mail: r.soualmi@univ-boumerdes.dz

Very recently, the application of LBM has been encouraged by many authors and has proved its suitability to simulate a large class of problems involving conductive, convective and radiative heat transfer. Mohamed and kuzmin [3] examined the natural convection phenomenon in square cavity using LBM. They evaluated the force term in the lattice Boltzmann equation. Double population thermal LBM with non-uniform mesh was applied by Dixit et al. [4] and Kuznik et al. [5] for the simulation of natural convection in square cavity. The authors found that it's required to implement the interpolation supplemented lattice Boltzmann method (ISLBM) [4] and the Taylor series expansion – and least square – based Lattice Boltzmann method (TLLBM) [5] in order to avoid the unreasonable use of high uniform lattice. Three-dimensional study of natural convection using lattice Boltzmann method was conducted by researchers in [6]. Li et al. [7] employed a Multirelaxation time model to simulate natural convection in a cubic cavity. Asinari and co-workers [8] applied the LBM to analyze the radiative equilibrium problem in 2D rectangular enclosure. Their work proved LBM's ability to solve the radiative heat transfer and was considered as the first step in this direction.

Very few researchers used hybrid schemes combining LBM and one of the CFD methods such as FVM and FDM to simulate natural convection problem. Zhengli et al. [9] coupled LBM and FVM to solve natural convection with different Rayleigh numbers, in which the velocity and the temperature fields were obtained using LBM and FVM respectively. They found an excellent agreement with the literature. Jami et al. [10] also applied a combined LBM and FDM to simulate laminar natural convection flows in a differentially heated square enclosure containing a heat-conducting cylinder. The limitation of FDM in solving problems with complex geometries led to a restriction on the development of FDM-LBM (although the biggest advantage of LBM is its applicability to solve the problems in a complex computational domain). The use of FVM in the other hand has been encouraged by many researchers, due to its completely conservative character and ability to overcome the FDM limitations.

In the literature, many researchers investigated the problem of coupled natural convection and volumetric radiation using traditional (CFD) methods to solve the momentum, energy and radiative transfer equations. Two-dimensional analysis of combined volumetric radiation and natural convection with participating medium, using S4 and S8 quadrature of discrete ordinates method (DOM), in square cavity was presented in [11] , while in Lauriat's work [12] , the problem was treated for a vertical cavity using P-1 approximation. It was commonly pointed out, in all the works mentioned above, that the flow and thermal fields were affected by the presence of radiation. Colomer et al. carried [13] out a natural convection and radiation phenomenon investigation in both transparent and participation medium in 3D differentially heated square cavity using DOM. They found that the heat flux increases with increasing Rayleigh number, while it decreases with increasing optical thickness, for the case of participating medium. Lui et al. [14] developed discrete ordinate-based method to study combined natural convection and radiation heat transfer in a square cavity containing an absorbing, emitting and scattering medium. They evaluated the effect of Rayleigh number, aspect ratio, optical thickness and scattering phase function on the behaviors of heat transfer. A numerical investigation of combined double diffusive and volumetric non-gray gas radiation in differentially heated square enclosure was conducted by Laouar-Meftah et al. [15] and it's 3D extension can be found in Cherifi's et al. study [16] . The influence of surface radiation and natural convection in differentially heated enclosures was also examined using different CFD methods [17] . The application of DOM has been very successful in solving the radiative transfer equation, and its accuracy and capability have been demonstrated in the study of Ramankutty and Crosbie [18] .

Different CFD/LBM combinations have also been employed to treat combined conduction or convection modes and radiation heat transfer. Transient conduction and radiation mode were tackled using the LBM for energy equation, along with a different CFD method for radiative equation such as FVM [19] and DOM [20]. Derfoufi et al. [21] numerically studied the mixed convection and volumetric radiation through a vertical channel using a combination of MRT-LBM, FDM and SRT-LBM to solve momentum, energy and radiative heat transfer equations respectively. They showed the efficiency of such combinations to simulate similar problems.

Only a few authors have used the LBM to compute all the macroscopic variables mainly velocity, the temperature and the radiative terms. Tighchi and Esfahani [22] demonstrated the suitability of LBM to examine the combined natural convection and volumetric radiation in square cavity containing a participating medium. Their study indicated that the results obtained purely with LBM needed shorter computational time than those obtained with LBM-FVM. A similar problem has been realized in square cavity with horizontal fin by Tighchi et al. [23]. The LBM has also proved its ability to investigate Rayleigh Benard convection with volumetric radiation problem in participating two-dimensional medium [24].

More recently, rarely research has been conducted on the study of coupled natural convection and volumetric radiation using certain LBM/CFD hybrid methods. Mondal and Mishra [25] incorporated uniform lattice with LBM and FVM to solve the combined natural convection and volumetric radiation in square cavity filled with an absorbing, emitting and scattering medium. They concluded that as long as the medium is more participating, the isothermal line would be condensed near the cold boundary. They later proceeded to do the same problem for the non-uniform lattice case, hence proving its efficiency, accuracy and computational time [26] . An interaction of Rayleigh Bénard convection and volumetric radiation using a hybrid method of the LBM with FVM was reported by Mishra et al.[27] . Chaabane et al. [28] also developed a new hybrid model to simulate combined natural convection and radiation phenomenon in 2-D square cavity filled with an absorbing, emitting and scattering medium. The temperature and the velocity fields were obtained using the two double population LBM, whereas the radiative term, in the energy equation, was computed using control volume FEM.

LBM-FDM combination along with DOM, although effective when incorporated together to treat coupled natural convection and volumetric radiation problems, are rarely encountered in the literature. Moufekkir et al. [29] made use of the hybrid thermal LBM to simulate natural convection and volumetric radiation in an isotropic scattering medium within a heated square cavity. The velocity and the temperature fields were computed using MRT-LBM and FDM respectively, while the radiative term was determined by DOM. They remarked that the centro-symmetrics of streamlines and isotherms was vanished in the presence of radiation.

To the best of our knowledge of the literature, the employment of the numerical combination of LBM-FVM with discrete ordinate method for the investigation of the combined natural convection and volumetric radiation in differentially heated

enclosure with different aspect ratio has not been considered yet. In this work, the velocity and the temperature fields were calculated by single relaxation lattice Boltzmann and finite volume methods respectively, while the radiative term in the energy equation was computed via the discrete ordinate method. The effect of Rayleigh number, optical thickness, aspect ratio and Planck number on the flow field, the temperature distribution, the velocity profiles and heat transfer was examined.

2. Problem Statement

The physical domain considered in the present work is sketched in figure 1. The vertical left and right walls are maintained at a uniform temperature T_h and T_c, respectively where $T_h > T_c$, while the horizontal walls are supposed adiabatic. The enclosure is filled with an absorbing, emitting and non-scattering gray medium. The two vertical walls are blacks ($\varepsilon_{1,2}=1$), whereas the two horizontal walls are reflective ($\varepsilon_{3,4}=0$). The fluid is incompressible and Newtonian. The flow is laminar, two dimensional and steady. All physical properties are constants except for the density, where the Boussinesq approximation is adopted. The effect of volumetric radiation is also considered to be present.

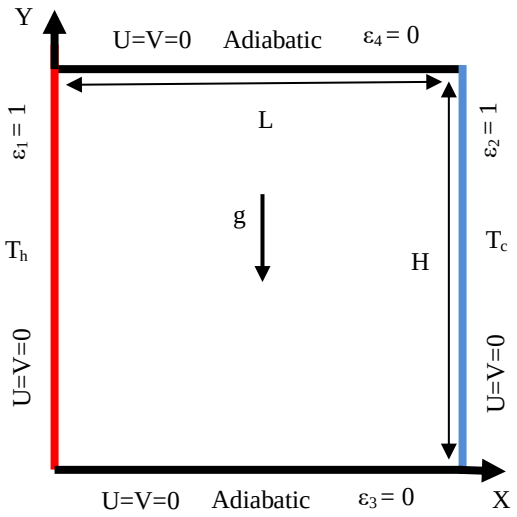

Figure 1. Scheme of the studied configuration

3. Numerical Simulation

The numerical implementation of LBM, FVM and DOM is presented in this section. As shown in figure 2, the fluid domain is discretized into uniform staggered lattices/control volumes. The SRT-LBM is used to simulate the velocity field at the lattices center, while the energy equation and the radiation source term, appearing in this equation, are solved at the same control volume nodes using FVM and DOM respectively. For both LBM and FVM/DOM approaches, we chose the same numbers of lattices/control volumes. The temperatures are computed at the center of FVM control volume. It is therefore necessary to calculate the temperatures' values at the center of lattices in order to introduce them in the buoyancy force term. Therefore, an average of temperature values at the control volume nodes surrounding the corresponding lattices' center is computed. For this reason, an interpolation between the LBM and the FVM was adopted. The average temperature at the lattice center is given as follows:

$$T_{avr}(i,j) = \left[T(i,j) + T(i,j+1) + T(i+1,j) + T(i+1,j+1)\right]/4 \qquad (1)$$

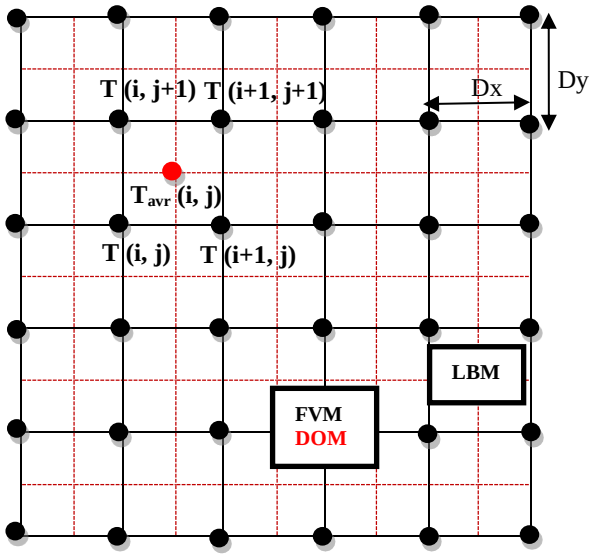

Figure 2. Arrangements of lattices in the LBM and control volumes in the FVM/DOM of the domain

In order to implement the velocity, found using the LBM, in the dimensionless energy equation, which is solved by the FVM, we have to convert the velocity in LB unit to a dimensionless velocity; therefore, the relationship between the LB and dimensionless velocities is given as:

$$U_{FV} = U_{LB}\,\frac{H}{\alpha} \qquad (2)$$

3.1. SRT lattice Boltzmann method for dynamics problem

The LBM is employed to solve the governing equations, which can be recovered from the lattice Boltzmann equation by using the Chapman Enskog analysis. In this work, The LBM simulates the movement of fluid particle by implementing the distribution function in order to compute the velocity field. The D2Q9 model has been adopted.

The LBM consists of two steps: streaming and collision. The collision step is regarded as a relaxation towards the equilibrium states. While the streaming process moves the fluid particle to the adjacent nodes according to their velocity and direction. The collision operator is linearized by the approximation of Bhatnagar-Gross-Krook (BGK) based on the single relaxation time (SRT).

To compute the flow field, the lattice Boltzmann equation, with external force after inserting the BGK approximation, can be written as:

$$\frac{\partial f_k(x,y,t)}{\partial t} + c_{kx}\frac{\partial f_k(x,y,t)}{\partial x} + c_{ky}\frac{\partial f_k(x,y,t)}{\partial y} = -\frac{1}{\tau_v}\left(f_k(x,y,t) - f_k^{eq}(x,y,t)\right) + F_k \qquad (3)$$

So the general form of the discretized LBM Eq. (3) can be expressed as:

$$f_k\left(x+c_{kx}\Delta t, y+c_{ky}\Delta t, t+\Delta t\right)= f_k\left(x,y,t\right)-\frac{\Delta t}{\tau_v} \left(f_k\left(x,y,t\right)- f_k^{\ eq}\left(x,y,t\right)\right)+\Delta t F_k \quad (4)$$

where $f_k(x,y,t)$ and $f_k^{eq}(x,y,t)$ are the distribution function and equilibrium density distribution function, respectively. Δt denotes the lattice time step, $\vec{c}_k$ is the discrete lattice velocity vector at the position (x,y) and the instant t. F_k and τ_v are an external body force in direction k and the lattice relaxation time, respectively.

The kinematic viscosity ν is related to the relaxation time τ_v :

$$\nu = c_s^{\ 2}\left(\tau_v - 1/2\right) \quad (5)$$

c_s is the lattice speed of sound . Note that the viscosity is required to be positive in order to avoid the numerical instability; therefore, the relaxation time should be superior to 0.5.

The discrete velocity is defined as follows:

$$\vec{c}_k = \begin{cases} c_0(0,0) & k=0 \\ c_k = c\left(\cos\left((i-1)\pi/2\right), \sin\left((i-1)\pi/2\right)\right) & k=1,2,3,4 \\ c_k = c\cos\left((i-5)\pi/2+\pi/4\right), \sin\left((i-5)\pi/2+\pi/4\right) & k=5,6,7,8 \end{cases} \quad (6)$$

For which $c_{kx}=\Delta x/\Delta t$ follows the *x* direction and $c_{ky}=\Delta y/\Delta t$ follows y direction, where Δx and Δy are the lattices spaces. In LBM units, Δx , Δy and Δt are equal to unity.

The Relationship between cs and ck for the arrangement D2Q9 is expressed as:

$$c_s = \frac{c_{k(x,y)}}{\sqrt{3}} \quad (7)$$

The local equilibrium distribution function $f_k^{eq}(x,y,t)$ is calculated by Eq. (8):

$$f_k^{\ eq}\left(x,y,t\right) = w_k \rho\left[1+\frac{c_k.U}{c_s^{\ 2}}+\frac{1}{2}\frac{\left(c_k.U\right)^2}{c_s^{\ 2}}-\frac{1}{2}\frac{U.U}{c_s^{\ 2}}\right] \quad (8)$$

where U and ρ are the macroscopic velocity vector (u,v) and density, respectively. w_k is the weighting factor which is given by:

$$w_k = \frac{4}{9} \quad k=0$$
$$w_k = \frac{1}{9} \quad k=1,2,3,4 \quad (9)$$
$$w_k = \frac{1}{36} \quad k=5,6,7,8$$

The last term in Eq. (4) needs to be included as follows:

$$F_k = F_{ky} = 3w_k\rho g\beta\left(T-T_0\right)c_{ky} \quad (10)$$

where β, g, ρ and T_0 are thermal expansion coefficient, gravitational acceleration, density and reference temperature respectively

The macroscopic quantities ρ , u and v were obtained from the expressions:

$$\rho(x,y) = \sum_k^9 f_k(x,y,t) \quad (11)$$

$$u(x,y) = \frac{1}{\rho(x,y)}\sum_k^9 c_{kx} f_k(x,y,t) \quad (12)$$

$$v(x,y) = \frac{1}{\rho(x,y)}\sum_k^9 c_{ky} f_k(x,y,t) \quad (13)$$

where c_{kx} and c_{ky} are the discrete velocity in *x* and *y* direction respectively.

3.1.1. Dynamics boundary conditions treatment

The hydrodynamic boundary conditions are modeled by the no-slip of fluid particles on all the solid walls, which translates to null at the boundaries. The boundary conditions used here are the same as those employed in [21] and are defined by the density distribution function. The Bounce back scheme was applied to determine the unknown velocity distribution function as shown in figure 3. In this scheme, the distribution functions of the particles are reflected to the fluid node in the opposite direction when the particles reach the solid walls. In general, the bounce back condition is given by the following rule:

$$f_{\bar{k}}(x_w,t) = f_k(x_w,t) \quad (14)$$

where x_w is a fluid node on the wall, and k and $\bar{k}$ represent two opposite lattice directions on boundary site.

For example, for the west and east walls, the unknown distribution functions can be written as follows:

$$f_5 = f_7 \qquad f_1 = f_3 \qquad f_8 = f_6 \quad (15)$$

$$f_7 = f_5 \qquad f_3 = f_1 \qquad f_6 = f_8 \quad (16)$$

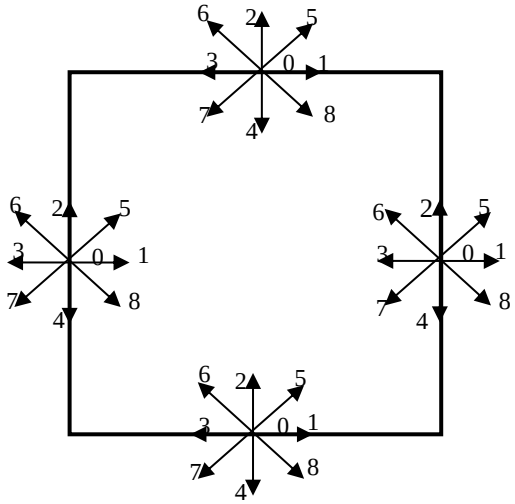

Figure 3. Boundary condition for D2Q9 model

3.2. Finite volume method for thermal problem

For the computation of temperature fields, the dimensionless energy equation with radiative source term can be expressed as follows [29]:

$$u\frac{\partial T}{\partial x}+v\frac{\partial T}{\partial y}=\left(\frac{\partial^2 T}{\partial x^2}+\frac{\partial^2 T}{\partial y^2}\right)+\frac{\Theta}{Pl}\nabla Q_R \tag{17}$$

where u and v, T and ∇Q_R are dimensionless, horizontal and vertical velocities, temperature and the divergence of radiative heat flux respectively.

The non-dimensional form of the above-mentioned equation can be obtained by using these dimensionless variables:

$$x=\frac{x^*}{H}\qquad y=\frac{y^*}{H}\qquad u=\frac{u^*}{\alpha/H}\qquad V=\frac{v^*}{\alpha/H}\qquad T=\frac{T^*-T_c}{T_h-T_c}$$

$$Q_R=\frac{q_R}{4\sigma T_0^3}\qquad \Theta=\frac{T_0}{T_h-T_c} \tag{18}$$

where, the superscript * indicates the dimensional variables.

The thermal field is treated using the finite volume method. The energy equation is discretized using a power law and a central difference scheme for the convective and diffusive term respectively.

3.2.1. Thermal boundary conditions treatment

The nondimensional boundary conditions can be obtained as follows:

- At the vertical walls:

On the left wall $T=T_h=0.5$ at $x=0$ and

$$0\le y\le H \tag{19}$$

On the right wall $T=T_c=-0.5$ at $x=L$ and

$$0\le y\le H \tag{20}$$

- At the adiabatic horizontal walls: the condition of adiabacity is obtained by Moufekkir et al.[29]:

On the bottom wall

$$-\left.\frac{\partial T}{\partial y}\right|_{y=0}=\varepsilon_3\frac{\Theta}{Pl}\left[\frac{1}{4}\left(1+\frac{T}{\Theta}\right)^4-\sum_{\xi_m<0}|\xi_m|\omega_m I_m(x,0)\right]\quad \text{at}$$

$$0\le x\le L \tag{21}$$

On the top wall

$$\left.\frac{\partial T}{\partial y}\right|_{y=H}=\varepsilon_4\frac{\Theta}{Pl}\left[\frac{1}{4}\left(1+\frac{T}{\Theta}\right)^4-\sum_{\xi_m>0}|\xi_m|\omega_m I_m(x,H)\right]\quad \text{at}$$

$$0\le x\le L \tag{22}$$

where ω_m is the quadrature weight for each direction. Θ is the reference temperature ratio ($\Theta=1.5$)

In this work, the horizontal walls are perfectly reflective, that is means that $\varepsilon_3=\varepsilon_4=0$. Thus, the condition of adiabacity on the bottom and the top walls respectively becomes, again as follows:

$$-\left.\frac{\partial T}{\partial y}\right|_{y=0}=0\qquad \text{at}\qquad 0\le x\le L \tag{23}$$

$$\left.\frac{\partial T}{\partial y}\right|_{y=H}=0\qquad \text{at}\qquad 0\le x\le L \tag{24}$$

3.3. Discrete ordinates method for radiative model

To obtain the divergence of radiative heat flux in Eq. (17), it is required to solve the radiative transfer equation (RTE). The non-dimensional form of RTE for a gray absorbing, emitting and no scattering medium, can be written as [29]:

$$\mu\frac{\partial I(x,y,\Omega)}{\partial x}+\xi\frac{\partial I(x,y,\Omega)}{\partial y}+\tau I(x,y,\Omega)=\frac{\tau}{4\pi}\left[1+\frac{T}{\Theta}\right]^4 \tag{25}$$

where ξ and μ are the direction cosines in y and x directions respectively. τ is the optical thickness that is equal to κL ($\tau=\kappa L$). κ is the extinction coefficient ($\kappa = a+\sigma s$). a and σs are the absorption and scattering coefficients, respectively (in this study, $\sigma s=0$). $I(x, y, \Omega)$ is the dimensionless radiation intensity in the direction Ω with $\Omega=\mu\vec{i}+\xi\vec{j}$

3.3.1. Radiative boundary conditions treatment

The dimensionless boundary condition for gray, diffuse and reflecting surfaces are given as:

- Left wall ($x = 0$):

$$I(0,y)=\frac{1}{4\pi}\left(1+\frac{T}{\Theta}\right)^4 \tag{26}$$

- Right wall ($x = L$):

$$I(L,y)=\frac{1}{4\pi}\left(1+\frac{T}{\Theta}\right)^4 \tag{27}$$

- Bottom wall ($y = 0$):

$$I(x,0)=\frac{1}{\pi}\sum_{\xi_m<0}|\xi_m|\omega_m I_m(x,0) \tag{28}$$

- Top wall ($y = H$):

$$I(x,H)=\frac{1}{\pi}\sum_{\xi_m>0}|\xi_m|\omega_m I_m(x,H) \tag{29}$$

The Discrete ordinate method has been used to solve the RTE associated with the above radiative boundary conditions, and the S8 quadrature has been adopted to discretize the angular space. Once the computation of RTE was performed, the radiation intensity for each direction in every position has been found. So the incident radiation and the divergence heat transfer are obtained as follows [29]:

$$G(x,y)=\int_{4\pi} I(x,y)d\Omega=\sum_{m=1}^{M}\omega_m I_m(x,y) \tag{30}$$

$$\nabla Q_R=\tau\left[\left(1+\frac{T}{\Theta}\right)^4-G(x,y)\right] \tag{31}$$

3.4. Heat transfer

The heat transfer is characterized, by the average convective, radiative and total Nusselt number along the active walls, which are defined respectively as follows:

$$Nu_{cv} = \int_0^H \left(\frac{\partial T}{\partial x} \right)_{x=0,L} dy \tag{32}$$

$$Nu_R = \frac{\Theta}{Pl} \varepsilon_{1,2} \int_0^H \left[\frac{1}{4} \left(1 + \frac{T}{\Theta} \right)^4 - Q^{inc}{}_{|X=0,L}(x,y) \right]_{x=0,L} dy \tag{33}$$

$$Nu_T = Nu_{cv} + Nu_R \tag{34}$$

where the emissivity of vertical walls is equal to the unity ($\varepsilon_1 = \varepsilon_2 = 1$). Q^{inc} is the incident radiation heat transfer, in which her expression is evaluated as follows:

$$Q^{inc}(0,y) = \sum\nolimits_{\mu_m<0} |\mu_m| \omega_m I_m(0,y) \tag{35}$$

$$Q^{inc}(L,y) = \sum\nolimits_{\mu_m>0} |\mu_m| \omega_m I_m(L,y) \tag{36}$$

4. Grid Independent Test and Code Validation

4.1. Grid Independent Test

The grid independency is tested by computing the total and radiative average Nusselt number on the heated wall for various lattice grids at Pr = 0.71, Pl = 0.02 , Ra = 10^6, Pr = 0.71, Θ = 1.5 and τ = 1. A converged solution is achieved when the maximum variation in horizontal and vertical velocities and temperature at any point reaches values under 10^{-5}. It seems from Table 1 that there is no significant change in NuT and Nur passing from 250×250 to 280×280. Therefore, a uniform grid size of 250×250 is chosen for the following work.

Table 1. The total and radiative average Nusselt number for different mesh sizes

Lattice size	Nu_T	Nu_r
80 × 80	34.82	30.58
100 × 100	34.80	30.43
150 × 150	34.74	30.22
200 × 200	34.70	30.11
250 × 250	34.67	30.03
280 × 280	34.67	30.01

4.2. Code Validation

In order to verify the reliability of SRTLBM-FVM combination to solve natural convection in conjunction with the DOM for volumetric radiation information, a comparison of our code's results with the numerical results of Yucel et al. [11], Moufekkir et al. [29] and Meftah et al. [15]was conducted. These results were compared for the average radiative Nusselt number at the hot wall for Ra =5 × 10^6, Pl = 0.02 and three optical thickness (0.2, 1 and 5) for Pr=0.71. It can be seen from Table 2, that a good agreement has been observed between the present results and those in [11, 15, 29] with a maximum discrepancy of 1.54 %.

5. Results and discussion

The numerical results obtained are presented in this section for the following variety of key parameters: the aspect ratio (Ar = 0.5- 1- 2), the Rayleigh number (Ra= 10^3 to 10^6), the optical thickness (τ = 0 - 0.2 - 0.5 - 5- 10- 30 -100) and the Planck number (Pl = 0.001-0.02-0.1-1-10-100) with Pr=0.71 and temperature ratio Θ = 1.5.

5.1. Streamlines, isotherms and velocity profiles

In this heading, we illustrate the corresponding streamlines and isotherms of the parametres detailed above. In order to understand the trend of streamlines, we proceed to plot the velocity profiles and present them in the figures below.

5.1.1 Effect of volumetric radiation and Rayleigh Number (Ra)

In what follows, we analyze the effect of different values of Ra on streamlines and isotherms in the absence and presence of radiation exchange. The simulations are performed for $10^3 \leq Ra \leq 10^6$, Pl =0.02, Ar =1 and τ =1. As shown in figure 4, in the absence of radiation, for low Ra (Ra= 10^3 and 10^4), the flow field is symmetrical and is characterized by a single cell structure. The corresponding isotherms are formed nearly parallel to the cavity wall, which implies that most of the heat is transferred by conduction. With increasing Ra to 10^5 then 10^6, the flow loses its symmetrical shape and a multicellular structure takes place. The isothermal lines are horizontal in the center of the cavity and are vertical near the hot and cold walls due to the thinning of boundary layers. The boundary layer becomes thinner and thinner for Ra=10^6 as a by-product of the important effect of buoyancy force in the enclosure. The stream function's values reached a maximum (|Ψmax|) for the above-mentioned Ra, of 1, 4.5, 9.4 and 15.5 respectively.

In the presence of volumetric radiation (τ =1), a circular cellular structure appears inside the enclosure for all Ra, but the shape and the intensity of the flow significantly changes and increases, respectively, with the Ra

For Ra=10^3 and 10^4, the streamlines have practically the same unicellular patterns as those in pure natural convection. However, the enclosure's core is shifted from the center to the lower right corner near the cold wall, and the values of stream functions in the other hand either increases (for Ra=10^4) or decreases (for Ra=10^3) significantly, especially in the core of the enclosure. The maximum values of stream function for both of the mentioned Ra are, respectively, |Ψmax| = 1 and |Ψmax| = 6. As for the isotherms, the radiation destroyed their inclination and made them purely parallel to the vertical active walls, which indicates that the heat is transferred mainly by conduction for Ra=10^3. In the case of Ra=10^4, where the buoyancy forces increases, the isotherms are slightly tilted with respect to the case of Ra = 10^3 due to the simultaneous effects of convection and radiation phenomenon. We can also observe a concentration of isothermal lines near the cold wall owing to the diffusion of the radiation into the cold wall, which causes a local increase of the temperature gradient for the two Ra mentioned.

Table 2. Comparison of radiative and total Nusselt number at the hot wall

Optical Thickness	Nusselt number and deviation	Current work	Yucel et al.[11]	Meftah et al.[15]	Moufekkir et al.[29]
τ =0.2	**Nu_R**	37.340	37.4	37.40	36.718
	%	----	**0.16%**	**0.16%**	**0.67%**
	Nu_T	45.895	46.11	46.05	45.509
	%	----	**0.47%**	**0.34%**	**0.85%**
τ =1	**Nu_R**	31.221	31.28	31.25	31.108
	%	----	**0.19%**	**0.093%**	**0.36%**
	Nu_T	38.625	38.93	38.81	38.725
	%	----	**0.78%**	**0.48%**	**0.26%**
τ =5	**Nu_R**	23.932	23.64	23.57	23.801
	%	----	**1.24%**	**1.54%**	**0.55%**
	Nu_T	31.576	31.76	31.59	31.778
	%	----	**0.58%**	**0.04%**	**0.64%**

As Ra increases to 10^5 and 10^6, the flow becomes considerably affected by the radiation, and the multicellular structure changes to a monocellular shape. The corresponding stream function maximums increase highly ($|\Psi max|$ = 29 and $|\Psi max|$ = 53) compared to those where the radiation is absent, which indicates an augmentation of the velocity in the presence of volumetric radiation. The temperature distributions are more influenced by the radiative exchange, which is shown by the disappearance of the stratification that existed in the enclosure's core (pure natural convection). The isothermal lines are more intensified near the cold wall, which causes an increase of local vertical temperature gradient mainly for $Ra=10^6$. This is due to the elevation in the fluid's absorption of the radiation. We can also remark a homogenization of the temperature in the enclosure. The effect of radiation on isotherms is more pronounced as Ra increases. We can concluded that the volumetric radiation greatly activates the heat transfer in the enclosure for a higher Ra. Similar findings have been noted by the author's work [29] , in which their analysis is only made for the cases of $Ra=10^6$ and $Ra=10^3$.

The velocity component's profiles, at the medians of the enclosure are presented in figure 5, and are compared, for the case of pure natural convection, with those obtained when radiation is present, at different Ra. For $Ra = 10^4$, it is observed that there is no influence of radiation on both U-velocity and V-velocity profiles. This is due to the insignificant of buoyancy force, hence the very low interaction of natural convection with radiation. However, for $Ra = 10^5$ and $Ra = 10^6$, the radiation exchange eliminated the symmetrical behaviour, that existed in the pure natural convection case, for both velocities' profiles, due to medium's absorption of heat, which caused the buoyancy force to rise. Therefore, velocities were amplified, engendered a higher circulation intensity in the enclosure (as confirmed in Figure 4). We can also remarked that, as Ra decreases, the gap between velocity profiles for both cases is lessened, due to the reduction of radiation effect.

5.1.2 Effect of optical thickness (τ)

To further highlight the effect of radiation on streamlines and isotherms, we consider various values of optical thickness ranging from 0 to 100 at $Ra=10^6$ and Pl = 0.02. As shown in figure 6, the streamlines and the isotherms are influenced by the rise in optical thickness, which indicates that the medium participates greatly. For τ = 0, the flow and thermal fields have the same patterns as that in the pure natural convection due to the medium's transparency. As the τ increases from 0.2 to 10, the multicellular flow changes gradually its shape to monocellular structure. For τ =10, the flow patterns show a development of the vortex in the enclosure's core, which tends to grow into pseudo multicellular structure again, with an increase of τ to 30 and 100. Thus, the strength of the flow circulation through the enclosure is increased where: $|\Psi max|$=15.4 at τ = 0, 21.8 at τ = 0.2, 33 at τ = 0.5 and 72 at τ = 5, and is decreased for the case of optical thickness of 10, 30, and100 where $|\Psi max|$ is equal to: 55, 31and 21.6 respectively. For thermal field, from τ = 0.2 to τ = 30, the patterns of isotherms are inclined in the center of the enclosure and more intensified near the cold wall, due to the medium's higher radiation absorption. This leads to an increase of the fluid's temperature in the enclosure. When τ exceeds 30, we can observe that the isotherms become stratified at the center of the enclosure and are therefore nearly similar to that of pure natural convection (τ = 0). The reason for this explain is that the fluid absorbs more heat, which leads the temperature difference to decrease between, the fluid and hot wall, and to increase between the fluid and the cold wall. As a result, the temperature difference between the vertical isothermal walls will increase, creating an intense natural convective motion. Due to the greater absorption of the medium with a very high optical thickness, the medium becomes more opaque, which implies an impossibility of any penetration of radiant energy into the enclosure's core and a higher elevation in temperature gradient near the active walls. Thus, the effect of radiation gradually disappears until pure natural convection state is reached.

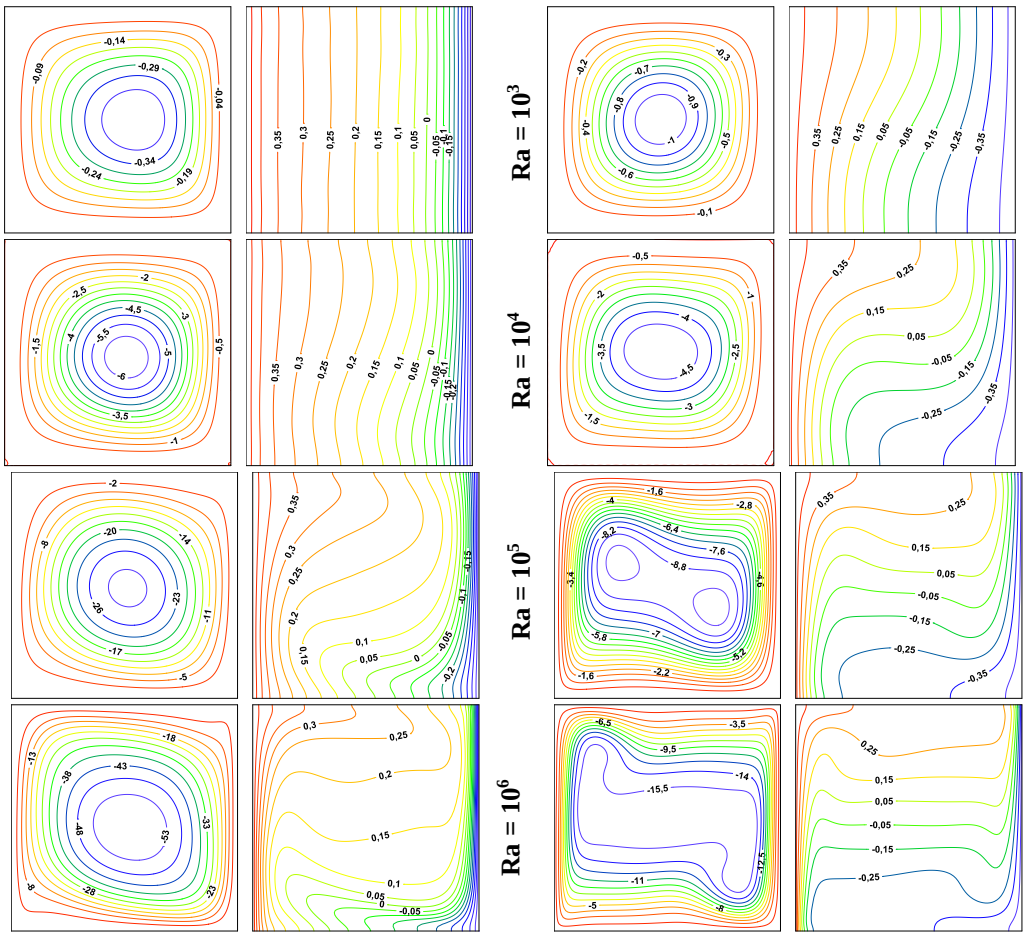

Figure 4. Streamlines (right) and isotherms (left) with different Ra

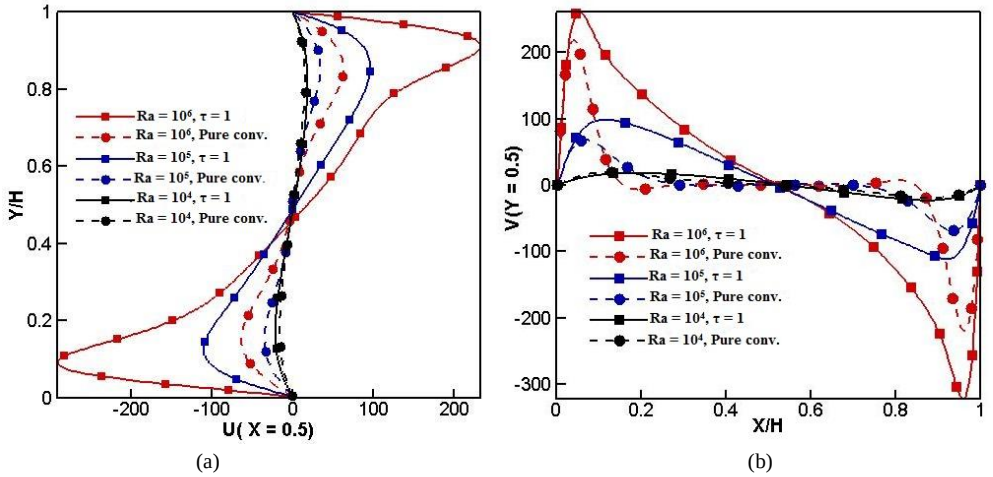

Figure 5. (a) U-velocity and (b) V-velocity profiles at X=0.5 and Y=0.5 respectively for different Ra

Figure 7 displays the effect of optical thickness on the U-velocity and V-velocity profiles for Ra=10^6 and Pl = 0.02. It can be seen that the effect is more intense when the optical thickness increases τ = 0 to τ = 5. The maximum and minimum velocity values have been noted in the case of τ = 5. However, by increasing the optical thickness from τ = 10 to τ = 100, both components of the velocity decrease due to the effect of radiation becoming negligible (the medium becomes nearly opaque). These observations confirm those found in term of streamline in figure 6.

5.1.3 Effect of Planck number (Pl)

In the following, we discuss the effect of Planck number ranging from 0.001 to 100, on the streamlines and isothermal lines for the case of τ = 1and Ra = 10^6. Looking at figure 8, a unicellular structure can be observed at low Pl (0.001 and 0.02). The same structure is elongated for the case of Pl=0.1. As Pl increases exceeds 1, the streamlines' patterns gradually take a shape similar to that of a natural convection problem. We can also notice that the stream function's values at the center of enclosure decrease with an increase in the Pl, where |Ψmax| is equal to: 203, 53, 22, 16, 15

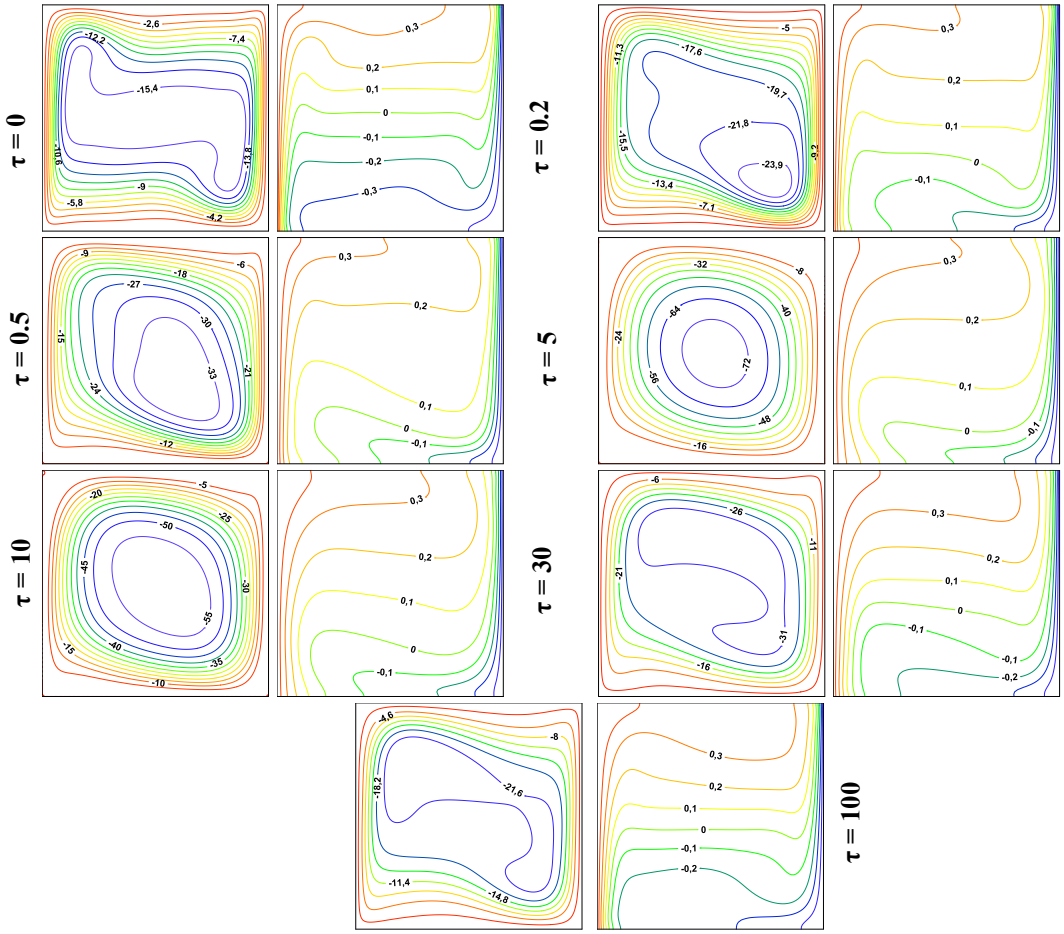

Figure 6. Streamlines (right) and isotherms (left) with different τ at Ra=10^6

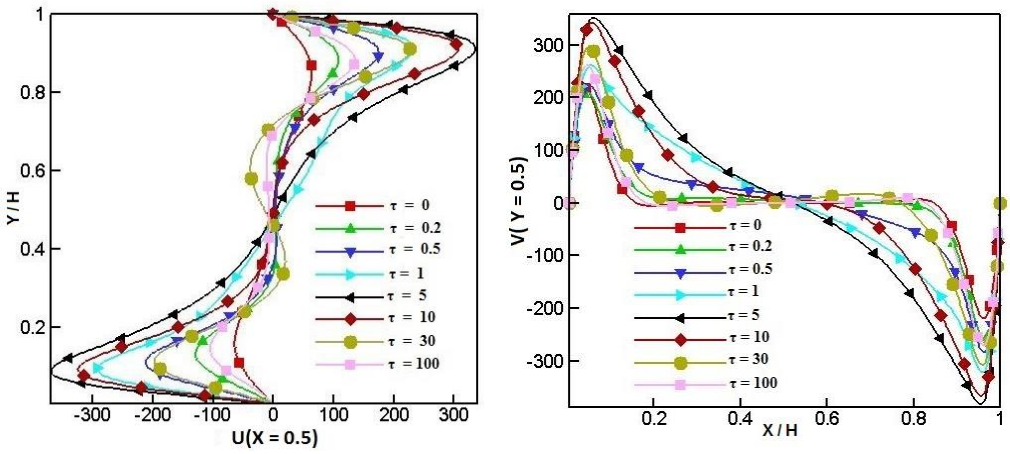

(a) (b)

Figure 7. (a) U-velocity and (b) V-velocity profiles at X=0.5 and Y=0.5 respectively for different τ

and 15 for Pl values of 0.001, 0.02, 0.1, 1, 10 and 100 respectively. This is due to the progressive attenuation of the radiation effect. As for the temperature distributions, it is visibly clear that the isotherms are no orthogonal to the adiabatic walls, and more condensed in the cold walls proximity, mostly for Pl=0.001, due to the higher temperature gradient resulting from the elevated radiation influence with respect to heat conduction regime. The isotherms only showed an inclination in the center of cavity starting from Pl=0.02, until the stratification was achieved for the case of Pl = 100, where a pure natural convection similar shape has been observed.

Figure 9 highlights the influence of Pl on the profiles of U-velocity and V-velocity, for Ra = 10^6 and τ = 1. It seems that the velocities' magnitude increases as Pl decreases. At the medians planes (X=0.5 and Y=0.5), these profiles are practically identical in behaviour for Pl ≥ 1 and Pl = 0.1, respectively. Therefore, we can safely conclude, that as Pl increases, its effect on velocity variations is insignificant.

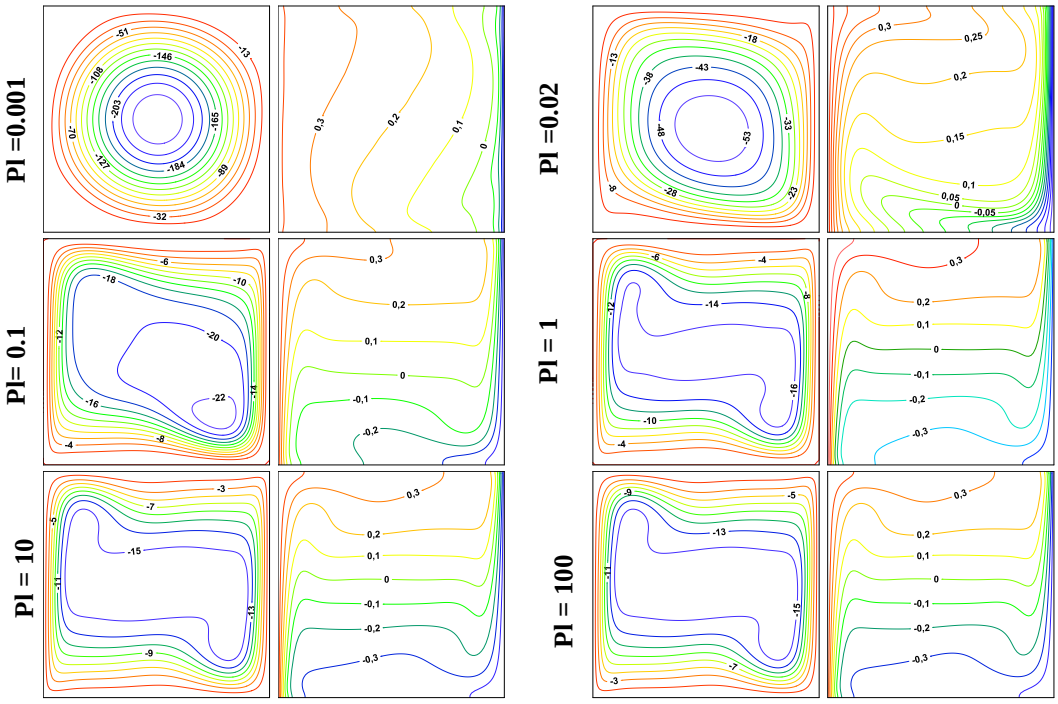

Figure 8. Streamlines (right) and isotherms (left) with different Pl at Ra=10^6

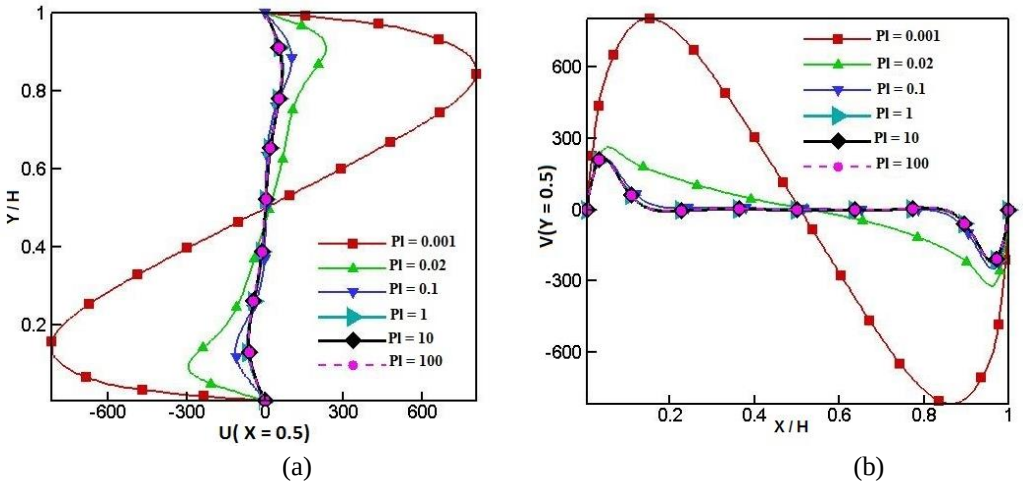

Figure 9. (a) U-velocity and (b) V-velocity profiles at X=0.5 and Y=0.5 respectively for different

5.1.4 Effect of aspect ratio (Ar)

Figure 10 illustrates the influence of aspect ratio on the streamlines and the isotherms at Ra=10^6, in the presence and absence of volumetric radiation, where $\tau = 1$ and Pl =0.02. The aspect ratio values considered are 0.5 (taller enclosure), 1 (square enclosure, their results is presented above in Figure 4) and 2 (shallow enclosure). It is clear that the radiation exchange for all Ar affected significantly the streamlines and the isotherms at higher Ra. As for flow field, in the presence of radiation, a clockwise rotating one-vortex structure, for all aspect ratios, has been observed. The maximum of stream function values at the center of the enclosure increases significantly with the increase in the Ar, thus indicating that the strength of air circulation becomes stronger when the enclosure configuration changes from the taller (Ar < 1) to the shallow (Ar > 1). However, for the case of radiation absence, the flow takes an elongated cell shape, which means a formation of a multicellular structure for all Ar (including Ar =1), and the increase in Ar doesn't affect the stream function's maximum in any significant way.

In the matter of the temperature distribution, the radiation exchange destroys the existing stratification (displayed in the case of the of lack radiation for all Ar) in the enclosure's center. Therefore, in the presence of radiation, for Ar = 0.5, it can be noticed that the isothermal lines are inclined in the core of the enclosure due to the existence of a low local horizontal temperature gradient , which indicates that, in addition to radiative heat transfer, there is a small transport of energy by conduction. This leads to slowing down the intense convective motion. As aspect ratio increases to 2, the inclination of these isotherm lines increases progressively until a pseudo stratification is created, thus the convective motion becomes more dominating. This is owed to the decrease of horizontal temperature gradient, and the increase of vertical temperature gradient close to the active walls, especially the cold wall. We can also observe an intensification of

isothermal lines closer to the cold wall for all aspect ratios because of radiation effect. We can conclude that the increase in Ar leads to a rise of thermal stratification inside the center of enclosure in the presence of radiation

The variations of U-velocity and V-velocity profiles for various Ar at Ra =10^6 and τ = 1 are illustrated in figure 11. The maximum and minimum values of both components of the velocity can be seen in the adiabatic and the isothermal walls, respectively, for the shallow enclosure (Ar =2). The loss of the symmetrical behavior in the two profiles of velocity is remarked as the Ar increases. The velocities' intensity for shallow enclosure is higher than that for the taller enclosure

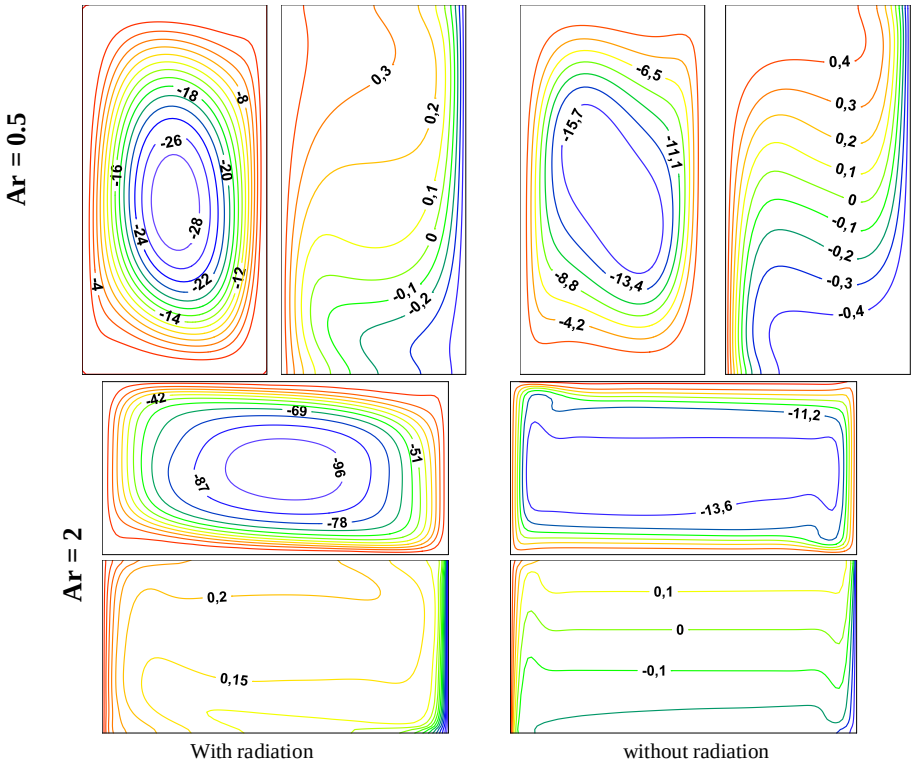

Figure 10. Streamlines and isotherms (right and left for Ar = 0.5, top and bottom for Ar=2) with different Ar at Ra=10^6

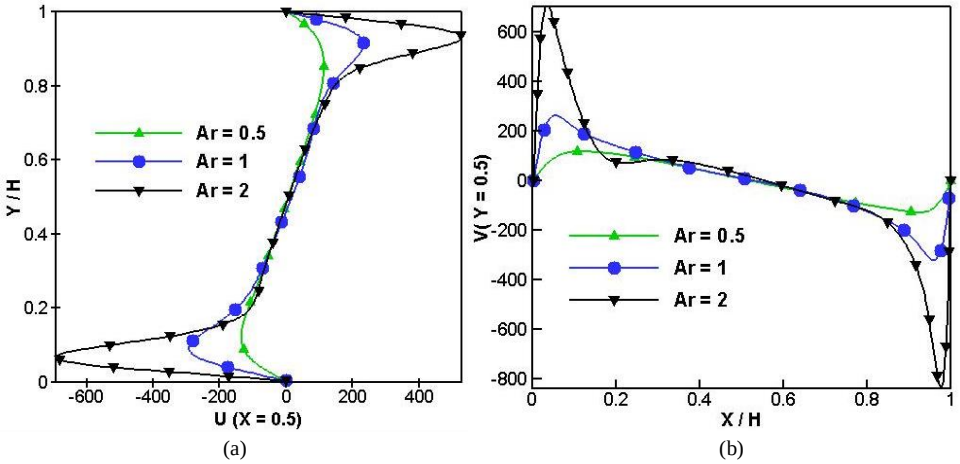

Figure 11. (a) U-velocity and (b) V-velocity profiles at X=0.5 and Y=0.5 respectively for different Ar

5.2. Heat transfer

Figure 12 illustrates the variation of average total Nusselt number along the hot wall with respect to aspect ratio, for low and high Ra (10^3 and 10^6), with the presence of radiation. The Nu_T decreases significantly with the increase of Ar for both Ra. At a given aspect ratio, it can also be observed that the Nu_T value is enhanced as Ra increases. This is because the buoyancy force effect becomes more significant in the enclosure.

In figure 13 and figure 14, the variation of total Nusselt number, along the heated wall, as a function of optical thickness and Planck number is displayed for Ra = 10^6. As shown in the figure 13, the Nu_T starts with a maximum value of 46.6 at τ = 0

(transparent medium), which corresponds to the maximum heat transfer, then decreases with the increase of the τ. Indeed, the higher of τ, the more heat is absorbed by the medium close to the heated wall and rises its temperature, which then makes optically thick. This is leads to a decrease in the radiative heat transfer on the heated wall.

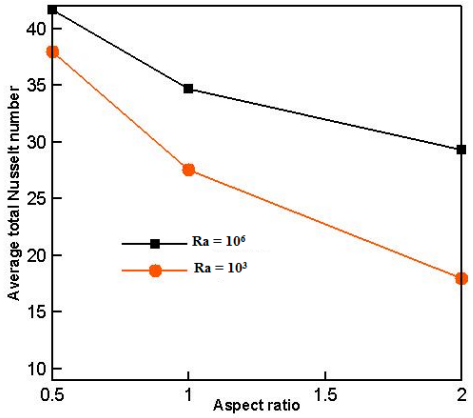

Figure 12. Variation of the average total Nusselt number as a function of Ar for Ra = 10^6 and Ra = 10^3

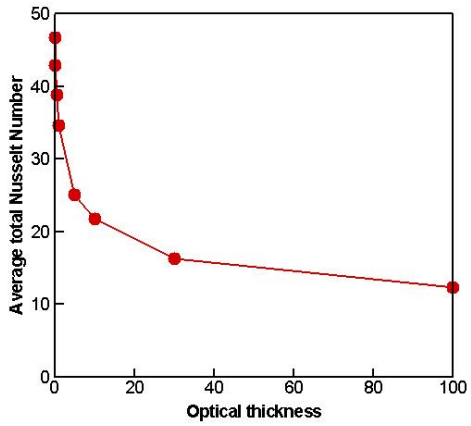

Figure 13. Variation of the average total Nusselt number as a function of τ for Ra = 10^6

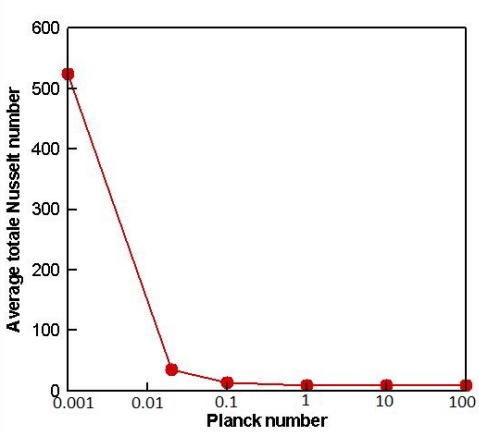

Figure 14. Variation of the average total Nusselt number as a function of Pl for Ra = 10^6

With regard to the figure 14, for τ = 1, the Nu_T decreases with the increase of the Pl from 0.001 to 0.1. While there is no considerable change in Nu_T values when Pl > 0.1. It can be seen that the Nu_T maximum value, Nu_T = 524, corresponds with Pl = 0. 001. This is due to the dominance of radiative heat transfer in low Pl.

6. Conclusion

In the present work, the combination of single relation time lattice Boltzmann and finite volume methods with discrete ordinates method was applied to simulate the coupled natural convection and volumetric radiative heat transfer. Some conclusions are listed below:

1. The aspect ratio has a pronounced effect on streamlines and isotherms in the presence of radiation. The strength of flow becomes higher when the shape of enclosure changes from slender (Ar < 1) to shallow (Ar > 1) and the isotherms become more inclined in the center of the enclosure.
2. The optical thickness' effect is only considered meaningful in a specific range of $0.2 \leq \tau \leq 5$.
3. As Planck number increases, the radiation effect on the streamlines and the isotherms diminishes progressively, until the pure natural convection pattern is obtained, especially from 1 to 100.
4. The velocity magnitude decreases with the reduction of the Plank number, but increases with the augmentation of Rayleigh number, optical thickness ($0 \leq \tau \leq 5$) and aspect ratio.
5. The average total Nusselt number along the hot wall decreases, in the case of Ra = 10^6 and Ra = 10^3, with the increase of aspect ratio.
6. The maximum value of the average total Nusselt number is obtained at τ = 0 and Pl= 0.001. An increase of Planck number and optical thickness causes a decrease in heat flux rate due to the diminution of the radiation effect.

Acknowledgments

This work was supported by a research grant (PRFU project: A05N01UN350120180002) from Direction Générale de la Recherche Scientifique et Développement Technologique (DGRSDT) (General Directorate of Scientific Research and Technological Development), Algeria

Nomenclature

c	Lattice speed		**Greek symbols**
c_s	Speed of sound	α	Thermal diffusivity
g	Gravitational acceleration	ν	Kinematic viscosity
ΔT	Temperature Difference	τ_v	Relaxation time
Δt	Time increment	ρ	Density
ΔX, ΔY	Lattice/ control volume spacing	W_k	Weighting factor
F	External forces	ω_m	Weight in each direction m
f	Density distribution functions	ε	Emissivity of wall
f_{eq}	Equilibrium density distribution functions	K	Thermal conductivity
I	Radiation intensity	β	Thermal expansion coefficient
G	Incident radiation	τ	Optical thickness
Q_R	Dimensionless radiative heat flux	μ, ξ	Direction cosines
q_R	Radiative heat flux	Ω	Direction vector
Q^{inc}	Dimensionless incident radiative flux	σ	Stefan-Boltzmann constant
H, L	Cavity height, cavity width	Θ	Reference temperature ratio
T_h	Temperature of the hot wall		
T_c	Temperature of the cold wall		**Subscripts**
T_0	Reference temperature	*	Dimensionless variables
u, v	Horizontal and vertical Velocity	0	Reference state
x, y	Cartesian coordinates	h	Hot wall
Ma	Mach number, $Ma=U/c_s$	c	Cold wall
Nu_{cv}	Average convective Nusselt number	t	Total
Nu_R	Average radiative Nusselt number	R	Radiative
Nu_T	Average total Nusselt number	LB	Lattice Boltzmann
Pr	Prandt number, $Pr = \nu/\alpha$	FV	Finite volume
Pl	Planck number, $Pl = K/(4H\sigma T_0^3)$		
Ar	Aspect ratio, (L/H)		
U	Characteristic velocity, $U=\sqrt{G\beta\Delta TH}$		
Ra	Rayleigh number, $Ra =(g\beta\,(T_h - T_c)\,H^3)/\alpha\nu$		

References

[1] A.A. Mohamad, 2011, Lattice Boltzmann Method: Fundamentals and Engineering Applications with Computer Codes, *Springer London* .

[2] S. Succi, 2011, The lattice Boltzmann equation: for fluid dynamics and beyond, *Oxford university press*.

[3] A.A. Mohamad, A. Kuzmin, 2010, A critical evaluation of force term in lattice Boltzmann method, natural convection problem, *International Journal of Heat and Mass Transfer*, (**53**) 990-996.

[4] H.N. Dixit, V. Babu, 2006, Simulation of high Rayleigh number natural convection in a square cavity using the lattice Boltzmann method, *International Journal of Heat and Mass Transfer*, (**49**) 727-739.

[5] F. Kuznik, J. Vareilles, G. Rusaouen, G. Krauss, 2007, A double-population lattice Boltzmann method with non-uniform mesh for the simulation of natural convection in a square cavity, *International Journal of Heat and Fluid Flow*, (**28**) 862-870.

[6] Y. Peng, C. Shu, Y.T. Chew, 2004, A 3D incompressible thermal lattice Boltzmann model and its application to simulate natural convection in a cubic cavity, *Journal of Computational Physics*, (**193)** 260-274.

[7] Z. Li, M. Yang, Y. Zhang, 2016, Lattice Boltzmann method simulation of 3-D natural convection with double MRT model, *International Journal of Heat and Mass Transfer*,(**94)** 222-238.

[8] P. Asinari, S. Mishra, R. Borchiellini, 2010, A Lattice Boltzmann Formulation for the Analysis of Radiative Heat Transfer Problems in a Participating Medium, *Numerical Heat Transfer, Part B: Fundamentals*, (**57**)126-146.

[9] Z. Li, M. Yang, Y. Zhang, 2014, Hybrid Lattice Boltzmann and Finite Volume Method for Natural Convection, *Journal of Thermophysics and Heat Transfer*, (**28**) 68-77.

[10] M. Jami, A. Mezrhab, M. Bouzidi, P. Lallemand, 2007, Lattice Boltzmann method applied to the laminar natural convection in an enclosure with a heat-generating cylinder conducting body, *International Journal of Thermal Sciences*, (**46**) 38-47.

[11] A. Yücel, S. Acharya, M.L. Williams, 1989, Natural Convection and Radiation in a Square Enclosure, *Numerical Heat Transfer, Part A: Applications*, (**15**) 261-278.

[12] G. Lauriat, 1982, Combined Radiation-Convection in Gray Fluids Enclosed in Vertical Cavities, *Journal of Heat Transfer*, (**104)** 609-615.

[13] G. Colomer, M. Costa, R. Cònsul, A. Oliva, 2004, Three-dimensional numerical simulation of convection and radiation in a differentially heated cavity using the discrete ordinates method, *International Journal of Heat and Mass Transfer*, (**47**) 257-269.

[14] X. Liu, G. Gong, H. Cheng, 2015, Combined Natural Convection and Radiation Heat Transfer of Various Absorbing-Emitting-Scattering Media in a Square Cavity, *Advances in Mechanical Engineering*, (**6**).

[15] S. Laouar-Meftah, D. Lemonnier, D. Saury, A. Benbrik, M. Cherifi, 2015, Comparative Study of Radiative Effects on Double Diffusive Convection in Nongray Air-CO2Mixtures in Cooperating and Opposing Flow, *Mathematical Problems in Engineering*, DOI 10.1155/2015/586913 (1-17).

[16] M. Cherifi, S. Laouar-Meftah, A. Benbrik, D. Lemonnier, D. Saury, 2015, Interaction of radiation with double-diffusive natural convection in a three-dimensional cubic cavity filled with a non-gray gas mixture in cooperating cases, *Numerical Heat Transfer, Part A: Applications*, (**69)** 479-496.

[17] S. Hamimid, M. Guellal, 2014, Numerical Study of Combined Natural Convection-Surface Radiation in a Square Cavity, *Journal of Thermophysics and Heat Transfer*, (**10**) 377-393.

[18] M.A. Ramankutty, A.L. Crosbie, 1997, Modified discrete ordinates solution of radiative transfer in two-dimensional rectangular enclosures, *Journal of Quantitative Spectroscopy and Radiative Transfer*, (**57)** 107-140.

[19] M.M. Keshtkar, P. Talebizadehsardari, 2018, Investigation of transient conduction–radiation heat transfer in a square cavity using combination of LBM and FVM, *Sādhanā*, (**43)**.

[20] Y. Sun, X. Zhang, 2016, Analysis of transient conduction and radiation problems using lattice Boltzmann and finite volume methods, *International Journal of Heat and Mass Transfer*, (**97**) 611-617.

[21] S. Derfoufi, F. Moufekkir, A. Mezrhab, 2018, Numerical assessment of the mixed convection and volumetric radiation in a vertical channel with MRT-LBM, *International Journal of Numerical Methods for Heat & Fluid Flow*, (**28**) 745-762.

[22] H. Ahmadi Tighchi, J.A. Esfahani, 2017, Combined Radiation/Natural Convection in a Participating Medium Using Novel Lattice Boltzmann Method, *Journal of Thermophysics and Heat Transfer*, (**31)** 563-574.

[23] H.A. Tighchi, M. Sobhani, J.A. Esfahani, 2018, Effect of volumetric radiation on natural convection in a cavity with a horizontal fin using the lattice Boltzmann method, *The European Physical Journal Plus*, (**133)**.

[24] S. Nataraj, K.S. Reddy, S.P. Thampi, 2017, Lattice Boltzmann simulations of a radiatively participating fluid in Rayleigh–Benard convection, *Numerical Heat Transfer, Part A: Applications*, (**72**) 313-329.

[25] B. Mondal, S.C. Mishra, 2008, Simulation of Natural Convection in the Presence of Volumetric Radiation Using the Lattice Boltzmann Method, *Numerical Heat Transfer, Part A: Applications*, (**55**) 18-41.

[26] B. Mondal, X. Li, 2010, Effect of volumetric radiation on natural convection in a square cavity using lattice Boltzmann method with non-uniform lattices, *International Journal of Heat and Mass Transfer*, (**53**) 4935-4948.

[27] S.C. Mishra, A. Akhtar, A. Garg, 2013, Numerical Analysis of Rayleigh-Bénard Convection with and Without Volumetric Radiation, *Numerical Heat Transfer, Part A: Applications*, (**65**) 144-164.

[28] R. Chaabane, F. Askri, A. Jemni, S. Ben Nasrallah,2017, Numerical Study of Transient Convection With Volumetric Radiation Using an Hybrid Lattice Boltzmann Bhatnagar–Gross–Krook–Control Volume Finite Element Method, *Journal of Heat Transfer*, (**139**).

[29] F. Moufekkir, M.A. Moussaoui, A. Mezrhab, H. Naji, D. Lemonnier, 2012, Numerical prediction of heat transfer by natural convection and radiation in an enclosure filled with an isotropic scattering medium, *Journal of Quantitative Spectroscopy and Radiative Transfer*, (**113)** 1689-1704.